REMOTE SENSING TECHNOLOGIES FOR EARTHQUAKE AND TSUNAMI DISASTER MANAGEMENT

Fumio Yamazaki and Masashi Matsuoka

ABSTRACT: This paper highlights the use of remote sensing technologies in disaster management, notably post-earthquake/tsunami damage detection due to the 2003 Bam Earthquake and the 2004 Indian Ocean Tsunami, and seismic risk assessment based on land use classification in Metro Manila, the Philippines. QuickBird (QB) images taken before and after the 26 December 2003 Bam Earthquake were used in visual damage interpretation based on the European Macroseismic Scale (EMS-98) building by building. An automated damage detection method was also applied to the post-event Ikonos and QB images. The results of these damage inspections were compared with field survey data and the accuracy and limitation of visual and automated damage detections were presented. QB images and GPS-synchronized photo/video were employed in the damage survey after the 2004 Indian Ocean Tsunami in the south Thailand. Terra-ASTER images were also used to identify tsunami inundation areas comparing the pre-event and post event images. For demonstrating the use of satellites images to urban classification, Landsat and Ikonos images were employed for Metro Manila. Using the normalized vegetation index and the texture of the image, a detailed classification of urban areas with respect to the density and height of buildings was sought. These examples show the usefulness of satellite images in disaster management.

KEYWORDS: the 2003 Bam Earthquake; the 2004 Indian Ocean Tsunami; satellite remote sensing; damage detection; seismic risk assessment

1. INTRODUCTION

In the recent few years, large scale earthquakes and tsunamis brought tremendous damages to urban and rural areas in the world, especially in Asia. It is also pointed out that rapid expansion of urban areas in developing countries has made the areas more vulnerable to various natural disasters. Thus, damage assessments before and after disasters have attracted significant attentions among researchers and practitioners of disaster management. Recent advancements in remote sensing and its application technologies made it possible to use remotely sensed imagery data for assessing vulnerability of an area and for capturing the damage distribution due to disasters.

To obtain pre- and post-event information on built and natural environment, several methods exist, such as field survey, airborne remote sensing, and satellite remote sensing. Because of its capacity to cover a vast area in one acquisition time, satellite remote sensing has been a very powerful tool to monitor the condition of the earth surface. High resolution satellite imagery, which has become available in the last few years, made satellite remote sensing more useful in disaster management since even damage status of individual buildings can be identified without visiting the sites of disasters.

In this paper, applications of satellite imagery to post-disaster damage detection are demonstrated for the 2003 Bam, Iran, earthquake and the 2004 Indian Ocean Tsunami. Application of satellite imagery for land use classification and seismic risk assessment is also presented for Metro Manila, the Philippines as an example.

2. THE 2003 BAM, IRAN, EARTHQUAKE

2.1 The Bam Earthquake and QuickBird Images

A strong earthquake of moment magnitude (Mw) 6.5 struck the southeastern part of Iran at 5:26:26 AM (local time) on 26 December 2003. The epicenter is located near the city of Bam in Kerman Province. According to the report of Iranian authority in June 2004, 26,271 people lost their lives, mostly due to the collapse of traditional mud-brick and clay houses, 30,000 people were injured and up to 75,600 people were left homeless (Relief Web 2004). About 85 percent of the housing and infrastructure have been destroyed in Bam. The United Nations estimates that the number of people affected by the loss of economic activity and damage to property and infrastructure is counted as 200,000. Arg-e-Bam, a historical citadel made by sun-baked mud-brick, was almost completely collapsed. The citadel was designated as World Heritage in Danger after the earthquake by UNESCO.

After the occurrence of the Bam earthquake, high-resolution commercial satellites observed the hard-hit areas: Ikonos on 27 December 2003, and QuickBird (QB) on 03 January 2004. The image of the Bam area was also captured by QB on 30 September 2003, about three months before the earthquake. The set of QB images are considered to be the second case acquired by civilian high-resolution satellites both before and after a severe earthquake disaster. The first case was the 21 May 2003 Boumerdes, Algeria, earthquake, and in that case, the images of Boumerdes City were taken about one year before, two days after and 28 days after the event, and those of Zemmouri City were obtained eight days before, two days after and 23 days after the event (Yamazaki et al. 2004).

In order to observe target areas in a short time interval, QB can change the view angle of its sensors. Thus, the two images of Bam have different off nadir view angles: 10 degrees (pre-event) and 24 degrees (post-event). Hence it is not so easy to superimpose these images exactly and to perform automated change detection. The difference in building

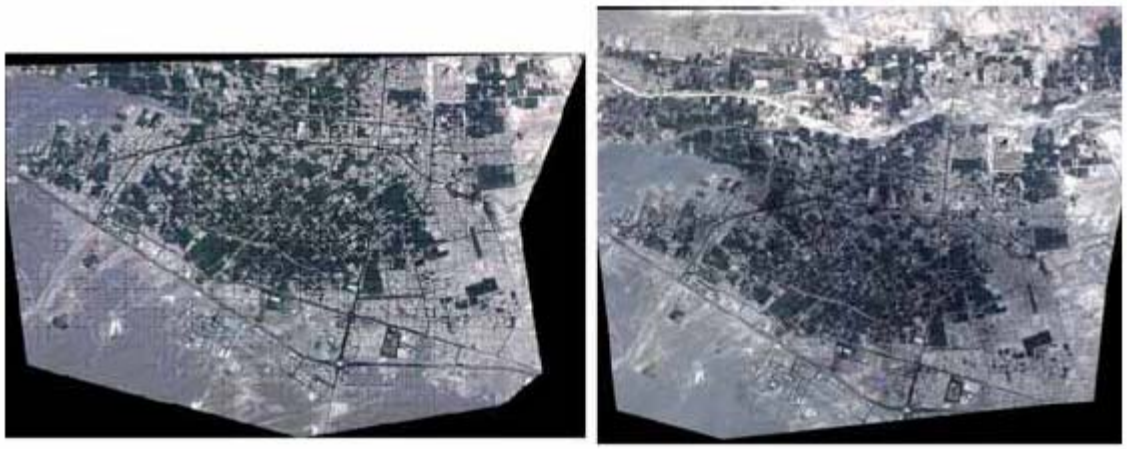

Figure 1. Pan-sharpened natural color QuickBird images of Bam City captured on 30 September 2003 (left: pre-event) and on 03 January 2004 (right: post-event)

shadow and vegetation in the different acquisition date images gives additional difficulty. Thus visual damage interpretation was performed first. Pan-sharpened images were produced by combining panchromatic images of 0.6m resolution and multi-spectral images of 2.4m resolution, as shown in Figure 1. By this image enhancement, buildings, cars and debris can clearly be seen.

2.2 Visual Damage Interpretation of Buildings

Using the pre-event image, the location of individual buildings was registered on GIS and city blocks surrounded by major roads were assigned. Then visual inspection of building damage was conducted based on the classification in the European Macroseismic Scale (EMS-98; European Seismological Commission 1998), shown in Figure 2. Comparing the pre- and post-event images, buildings surrounded by debris (Grade 3), partially collapsed buildings (Grade 4) and totally collapsed buildings (Grade 5) were identified.

In Figure 2, typical pre- and post-event QuickBird images for houses classified as Grades 3, 4, and 5 by visual inspection are also shown. Because the spatial resolution of the image is around 0.6m, it is almost impossible to detect damage equal to or less than Grade 2. It is rather easy to detect Grade 5 damage and in agreement among different interpreters was good in case of Grade 5 (Yamazaki et al. 2004). The effects of shadow and vegetation in damage classification become more serious for Grade 4 and damage detection becomes more difficult than that for Grade 5. Damage becomes even more difficult to detect for Grade 3, especially from vertical images. If some deformation is located on the roof or some debris spreads around a building, Grade 3 damage can still be identified.

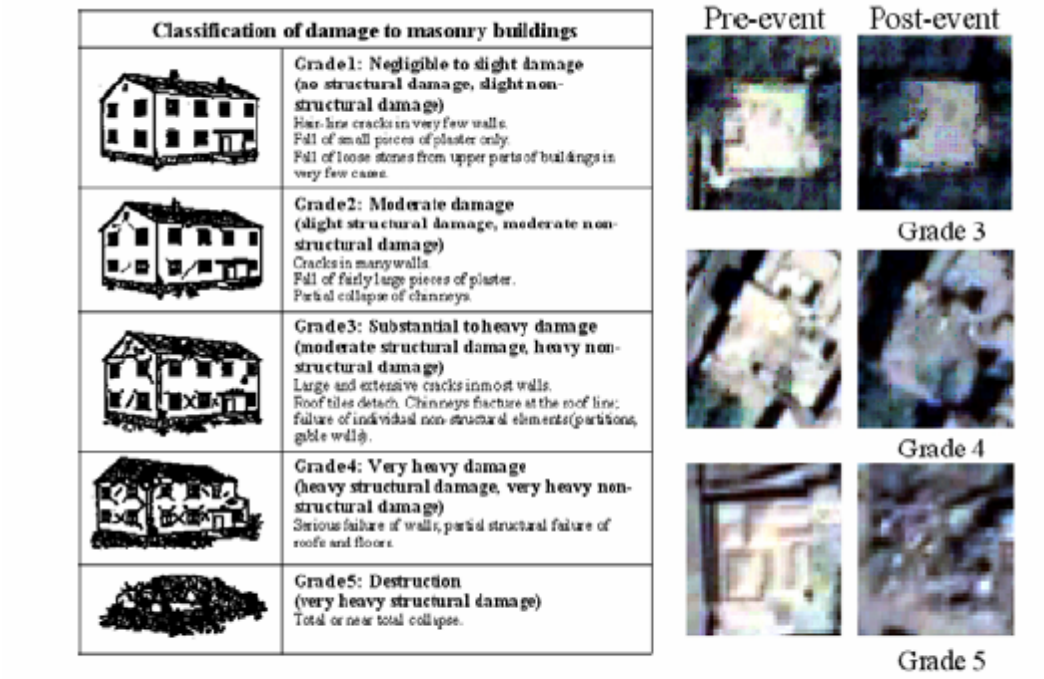

Figure 2. Classification of damage to masonry buildings (EMS 1998) and typical pre- and post event QuickBird images for Grades 3, 4 and 5 houses

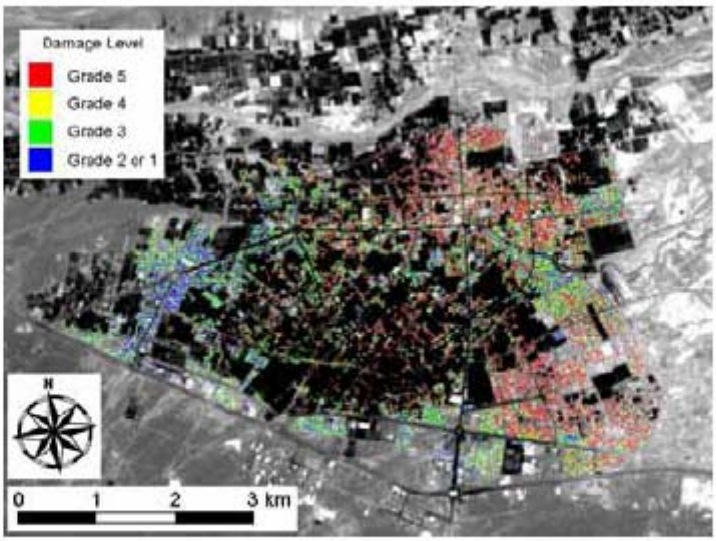

Figure3. Result of visual damage interpretation using QuickBird images acquired on 30 September, 2003 and 3 January, 2004. Damage levels are based on EMS-98

QuickBird \ Field survey	G 1	G 2	G 3	G 4	G 5	sum
G 1 & G 2	0	0	0	0	0	0
G 3	0	2	2	1	4	9
G 4	0	1	2	1	5	9
G 5	0	0	3	2	27	32
sum	0	3	7	4	36	50

Figure 4. Result of our visual interpretation compared with field survey data by Hisada et al. (2005) around aftershock seismic station No. 1, located in the south of Arg-e-Bam

By this visual interpretation using the pre- and post-event images, a total 12,063 buildings were classified building by building (Yamazaki et al. 2004), based on their damage grades, as depicted in Figure 3. The numbers of identified damaged buildings are 1,597 (Grades 1 or 2: blue points), 3,815 (Grade 3: green), 1,700 (Grade 4: yellow), and 4,951 (Grade 5: red). The time elapsed to register the location of individual buildings and city blocks using the pre-event image was around 30 hours, and judging and registering the damage grade of each building using the pre- and post-event images was around 20 hours. These elapsed times are considered to be highly dependent on the number of buildings, quality and resolution of images, and experience and efficiency of interpreters.

To examine the accuracy of damage detection in Bam, the field survey data by Hisada et al. (2005) was employed. They used the same EMS-98 scale to describe the damage grade of each building near eight aftershock recording stations, which were established

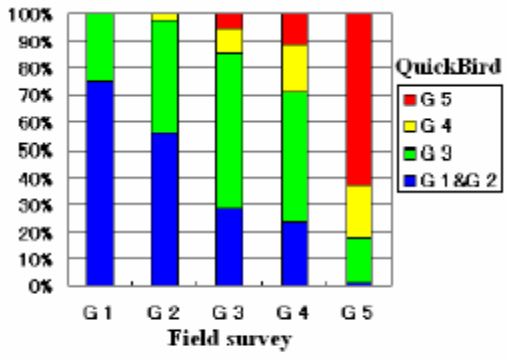

QuickBird \ Field survey	G 1	G 2	G 3	G 4	G 5	sum
G 1 & G 2	12	50	29	15	2	108
G 3	4	37	57	30	25	153
G 4	0	2	10	11	30	53
G 5	0	0	10	7	95	107
sum	16	89	101	63	152	421

Figure 5. Comparison of the result of the field survey around 6 aftershock observation sites in Bam City and that of our visual damage interpretation.

by International Institute of Engineering Earthquake and Seismology (IIEES). Figure 4 shows the satellite image and our visual inspection result around the aftershock seismic station No. 1, together with the cross table between Hisada's survey and our result. Each cell (row, column) in the table shows the number of buildings judged as Grade x (row) in visual interpretation and classified as Grade y (column) in field survey. This area is located in the south of Arg-e-Bam. Sixteen houses were made of mud brick (adobe), and 30 houses were of simple masonry construction. The damage ratio for Grade 5 is 72% by Hisada's survey while it was 64% in our visual inspection. The coincidence of damage grade between the two data sets is quite high in this area.

Figure 5 summarizes the comparison of the result of the field survey around six aftershock observation sites (421 buildings total) in Bam City and that of the visual damage interpretation. Commission errors (judging damage as higher grades than the field survey result) are seen in the cross table. But only 16 buildings were interpreted as more than one grade higher. Thus, commission error can be judged as not so significant as for quick-look damage detection. Omission errors: judging Grade 4 damage as Grade 1-3, and judging Grade 5 damage as Grade 1-4, are also seen in the cross table. Forty-two buildings were interpreted as less than one grade lower. It may be concluded that we should expect some amount of omission error in damage detection from optical higher solution satellite images, and thus we should consider this fact in estimating damage statistics at an early stage.

2.3 Automated Damage Detection

Visual damage interpretation using high-resolution satellite images is reliable but time consuming as stated above. Hence, application of the automated damage detection method developed by Mitomi et al. (2002) was sought. This method was first applied to aerial television images taken after the 1995 Kobe, Japan, the 1999 Kocaeli, Turkey, the 1999 Chi-chi, Taiwan, and the 2001 Gujarat, India, Earthquakes (Mitomi et al. 2000, 2001). The uniqueness of this method is highlighted by the fact that only a post-event image is used to characterize the debris of buildings.

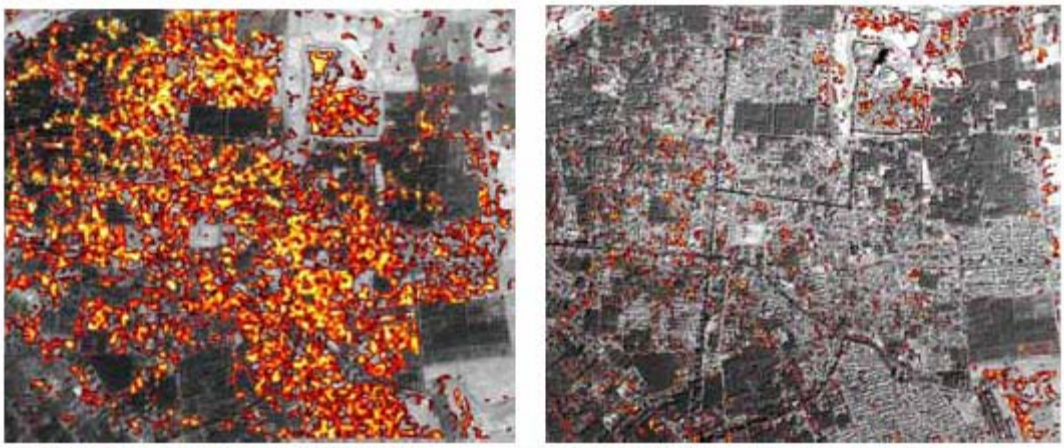

(a) Ikonos image taken on 2003/12/27 (b) QuickBird image taken on 2004/1/03

Figure 6. Results of detected areas with damaged building for original pan-sharpened images.

Areas with building damage are defined by color indices and edge intensities calculated from original RGB (red, blue, green) images. However, it is difficult to apply the same threshold values used for the color indices to other images due to the differences in factors such as the amount of sunlight and local environments. Thus, we proposed an area-independent technique (Mitomi et al. 2002) to estimate the areas with damaged buildings using edge information in local windows, such as edge variance and edge direction, and statistical textures derived from the co-occurrence matrix of the edge intensity. The details of the method are described in Vu et al. (2005a).

Figure 6 shows the results of the damage detection method applied to the Ikonos and QB images of central Bam. Vegetated areas were removed by thresholding the NDVI (Normalized Difference Vegetation Index). According to the visual damage inspection from QB images in the previous section and the reconnaissance field survey by Hisada et al. (2004), more than 80% of buildings in the south of Arg-e-Bam were classified as Grade 4 or 5 in EMS-98 scale. The distribution of detected damage from Ikonos is consistent with these results. However, less damage area was detected from the QB image. Spatial resolution and color distribution might be main factors that affect the results.

A re-sampled, one-meter resolution QB image provided a similar result as the original QB image. Hence, spatial resolution is not the reason of the difference. We also calculated the rations of digital numbers (DNs) of green and blue to that of red in the pan-sharpened images to examine the effects of color. The average rates of green and blue to red values were 0.97 and 0.95 for Ikonos while 1.03 and 1.14 for QB, which implies that the QB image is predominantly cyan. In fact, the original QB image does not look natural, but has a blue tint. Therefore, the color of the QB image was modified by histogram matching with the Ikonos image.

Figure 7(a) shows the results of damage detection using the color-modified QB image and the detected result from the color-modified QB image is similar to that from the Ikonos image. Thus, the detection is mainly influenced by the color distribution among

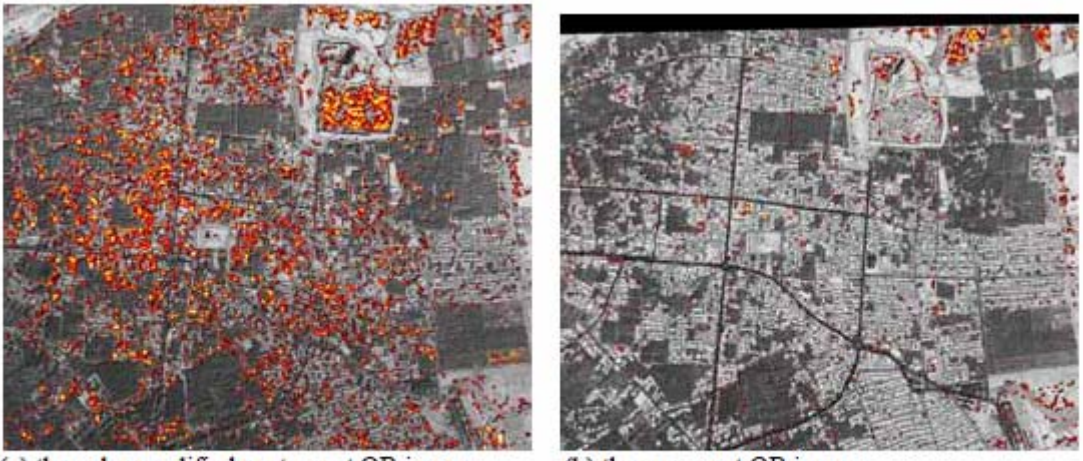

(a) the color-modified post-event QB image (b) the pre-event QB image

Figure 7. Distribution of detected damage areas using (a) the color-modified post-event QB image and (b) the pre-event QB image

red, green, and blue channels. Comparing the automated damage detection results from the post-event QB and Ikonos images with that from visual inspection and the field survey data, the damage distributions seem to agree reasonably well among them.

The automated damage detection method was further applied to the pre-event QB image. As seen in Figure 7(b), the detected building damage areas (noise) are limited to only small portions on the image. Hence, the commission error by the present automated damage detection method can be judged to be small. In the present example, we could use the Ikonos image as a reference to modify the color tone of the QB image. But this situation is not expected in the most cases. Hence, the proposed automated damage detection method still needs to be enhanced to obtain more stable and reliable results in various situations.

3. THE 2004 INDIAN OCEAN TSUNAMI IN SOUTH THAILAND

3.1 The 2004 Indian Ocean Tsunami and Field Survey in Thailand

A moment-magnitude 9.0 earthquake struck the area off the western coast of northern Sumatra on 26 December 2004. The magnitude is registered as the forth among the earthquakes worldwide after 1900. This gigantic earthquake triggered massive tsunamis, which inundated coastal areas in countries all around the Indian Ocean rim – from Indonesia to East Africa. Tsunami related deaths have been reported in 11 countries, including Indonesia, Sri Lanka, India, Thailand, Malaysia, Myanmar, Maldives, Bangladesh, Somalia, Tanzania and Kenya. The death toll including missing is approximately 280,000 according to United Nations and governments (Relief Web 2005).

In Thailand, the provinces facing Andaman Sea, notably, Phang-Nga, Phuket, and Krabi, were attacked by repeated tsunamis. The death toll in Thailand reached 5,395 and 2,932 people were listed as missing as of 09 March 2005. Nearly half of those confirmed deaths, and half of those missing were foreign tourists who were spending their holiday season in the resort areas.

As the scale of this tsunami disaster became unveiled, the present authors have decided to form an international survey team to gather geo-referenced tsunami inundation and damage information with the enhance use of satellite images and GPS. A similar joint survey team supported by Earthquake Disaster Mitigation Research Center (EDM), Japan, and the Multidisciplinary Center for Earthquake Engineering Research (MCEER), USA, was formed after the 1999 Kocaeli, Turkey earthquake for the first time (Eguchi et al. 1999; EDM 2000). The joint reconnaissance survey was also conducted after the 2004 Mid-Niigata earthquake. It was almost impossible to cover the large tsunami-affected areas by a small group. Thailand was selected as our primary survey area because of existing research collaboration and accessibility to the sites at an early stage. Geo-Informatics and Space Technology Development Agency (GISTDA), Thailand, provided various satellite images for this joint survey.

Figure 8(a) shows the members of the international survey team. The team was formed by Chiba University (Japan: F. Yamazaki), EDM (Japan: M. Matsuoka), ImageCat Inc./MCEER (USA: S. Ghosh), Asian Institute of Technology (Thailand: P. Warnitchai), GISTDA (Thailand: S. Polngam and S. Lawawirojwong), and Japan International Cooperation Agency (Japan: M.

Honzawa). The primary objective of our survey is to gather geo-referenced tsunami inundation and damage information, and hence we brought several digital video cameras and digital still cameras. Figure 8(b) shows a scene of geo-referenced video shooting using three video cameras. The field survey was carried out from 8 to 11 January 2005, covering hard-hit areas, e.g. Khao Lak, Phuket Island, Phi Phi Island. Please refer the survey reports in Ghosh et al. (2005) and Yamazaki et al. (2005).

Figure 9 shows the post-tsunami Ikonos images of Khao Lak and photos taken during the field survey. Blue dots in Ikonos images are the location of geo-referenced photo shooting. Figure 9(a) is Ikonos image of Phakarang cape area with 1m resolution, (b) is the photo of devastated Bamboo Orchid Resort on Phakarang cape, (c) shows a car thrown on the roof by tsunami. If we enlarge the Ikonos image, several black pixels corresponding to this car can be identified. Figure 9(d) is Ikonos image of mid Khao Lak

Figure 8. (a) Members of the international survey team and (b) panorama-VIEWS shooting in the field survey of south Thailand by 3 videos

Figure 9. Post-tsunami Ikonos image of Khao Lak and photos taken during the field survey. Blue dots show the location of geo-reference photo shooting. (a) Phakarang cape area, (b) devastated Bamboo Orchid Resort on Phakarang cape, (c) a car on the roof, (d) mid Khao Lak area near Weather Station, (e) a collapsed bridge by tsunami, (f) destroyed cottages in a resort, (g) Nang Thong Beach area in lower Khao Lak, (h) & (i) Similana Resort devastated by tsunami

and (f) shows destroyed cottages in a resort. Figure 9 (g) shows Nang Thong Beach area in lower Khao Lak, and Figures 9(h) and (i) are photos taken in Similana Resort, which was devastated by tsunami of about 5m high.

3.2 Panoramic VIEWS: GPS Synchronized Multiple Video Shooting

VIEWS (Visualizing the Impacts of Earthquakes With Satellites) has been developed by ImageCat, Inc. with the financial support from MCEER. VIEWS is a notebook-based system, which integrates GPS-registered digital video footage, digital photographs and observations with high-resolution satellite imagery, collected before and after a disaster (Adams et al. 2004). VIEWS was previously used in reconnaissance activities following the 2003 Bam, Iran earthquake, the 2004 Hurricanes Charley and Ivan that hit the Mexico Gulf coast of USA, and the 2004 Mid-Niigata, Japan earthquake.

In this tsunami survey in Thailand, the field-based damage assessment was conducted using VIEWS. These ground-based observations can be later used to validate damage characteristics identified on satellite imagery. It is envisioned that such perishable data will be invaluable for

future research in evaluating damage from tsunami hazards. We brought several video cameras in our field survey in Thailand. Thus, a new data collection approach was adopted (Figure 8(b)) by deploying three video cameras that simultaneously captured footage for three directions (front, left, and right) in some heavily affected areas. This streamlined the video collection process and provided a wider view of the area. We named this new system as "Panoramic-VIEWS".

In order to integrate, share, visualize, and ultimately analyze post-disaster reconnaissance field data collected using VIEWS, MCEER funded the development of tandem internetand desktop-based "virtual reconnaissance systems" (Ghosh et al., 2005). Figure 10 shows a screen shot from the virtual reconnaissance system, showing satellite imagery (Ikonos on 2004/12/29) with GPS readings and video footage from three video cameras collected in Khao Lak. Users have an option to toggle between multi-temporal and multi-source satellite images, and to explore these images in detail using zoom in and zoom out functions. These images are overlaid with GPS routes collected during the survey. By selecting a GPS point, users can view corresponding video footage and scroll the photographic archive in the adjacent windows.

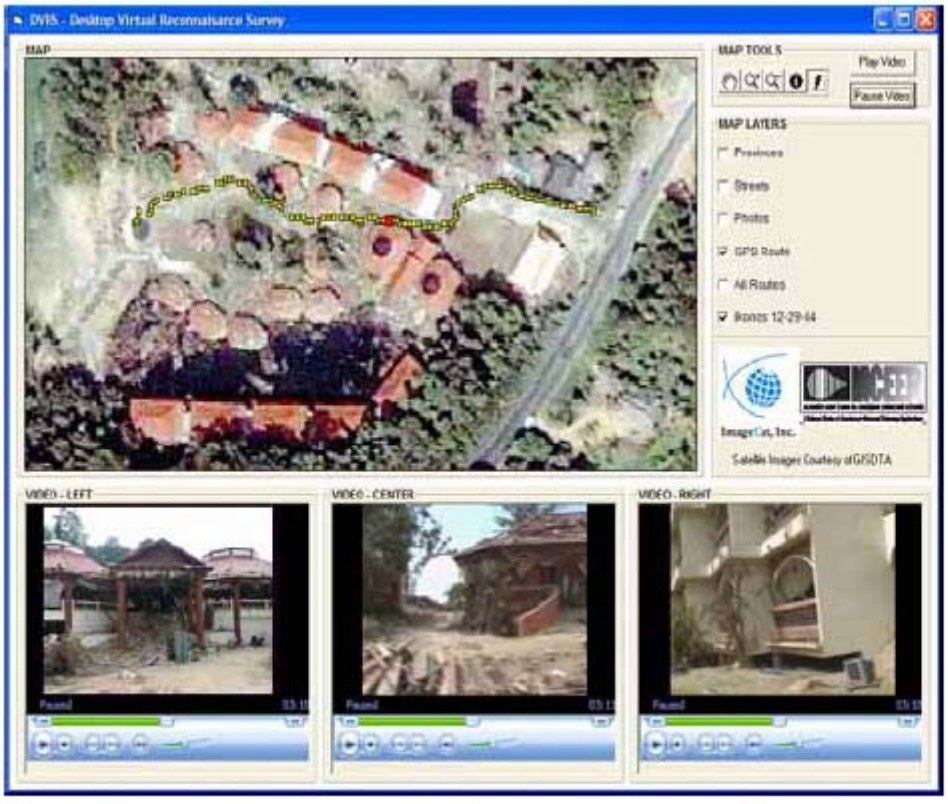

Figure 10. Screen shot from the virtual reconnaissance system (D-VRS), showing satellite imagery (Ikonos on 2004/12/29) with GPS readings and video footage from three video cameras collected in Khao Lak, Thailand

3.3 Tsunami Inundation Mapping Using Terra-ASTER Images

In the Indian Ocean Tsunami Disaster, various satellites observed the affected areas after the tsunami, and some of them have archive images before the tsunami. ASTER (Advanced Spaceborne Thermal Emission and Reflection Radiometer) is one of the sensors on board Terra satellite (Yamaguchi et al. 1998). The visible and near infrared radiometer of ASTER produces imagery of ground sampling interval of 15m, and it has the three nadir-looking bands and one backward-looking band for stereo scoping. Unlike other optical sensors, ASTER does not have a blue color band.

Terra-ASTER observed the hard-hit area including Khao Lak two years before and 5 days after the tsunami, as shown in Figure 11 in false color: which means the reflectance of the near-infrared (NIR) band is assigned to the red component, that of the red (R) band to the green component, and that of the green (G) band to the blue component, respectively. The false color images are shown by overlying on a digital elevation model of 90m grid from SRTM (Shuttle Radar Topography Mission, Jet Propulsion Laboratory (2005)).

Comparing these images, it could be observed that the reflectance of the near-infrared band in the affected areas became weak after the tsunami, which roughly means that, due to the tsunami, vegetation there might be removed/killed and that the land cover class might be changed to soil. This observation has also been confirmed in the field survey.

ASTER sensor can collect the data of not only visible and near-infrared bands but also a short wavelength infrared (SWIR) band. The resolution is 15m for visible and near infrared bands and 30m for SWIR band. Hence, ASTER data with moderate-resolution is

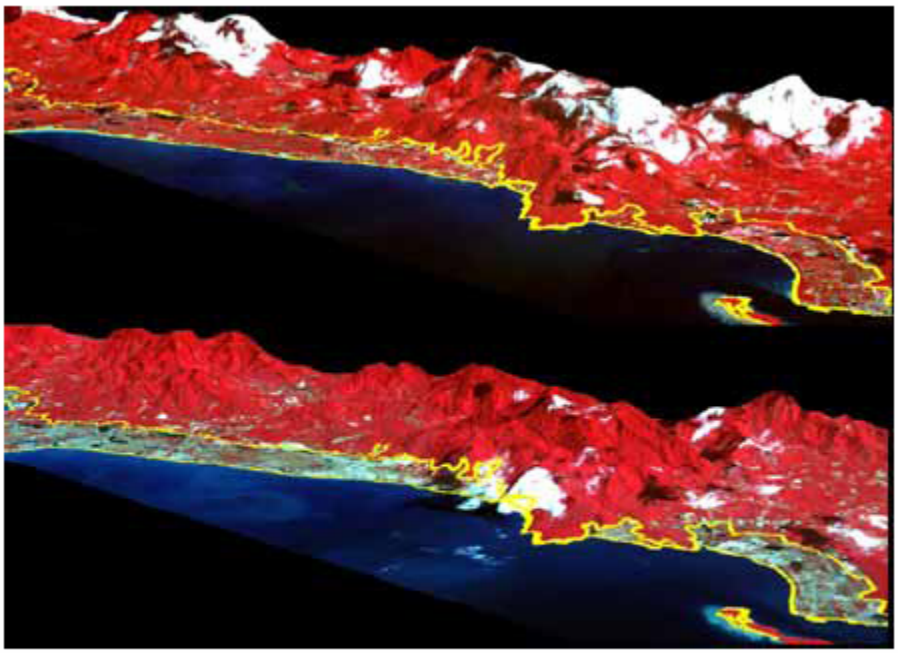

Figure 11. False color ASTER images of Khao Lak on 2002/11/15 (top) and on 2004/12/31 (bottom) overlying on SRTM 90m DEM. Yellow lines indicate the tsunami affected boundary, detected from Ikonos images by Vibulsreth et al. (2005).

useful for detecting wide tsunami inundation areas quickly because red, near-infrared and short wavelength infrared bands are considered to give the good indicators of land cover characteristics and, in fact, the normalized difference vegetation, soil and water indices have been proposed using these three bands (Takeuchi and Yasuoka 2004). From the reflectance of the red (R), near-infrared (NIR), and short wavelength bands (SWIR), the normalized difference vegetation (NDVI), soil (NDSI) and water (NDWI) indices can be calculated by Equations 1-3.

$$NDVI = (NIR - R) / (NIR + R) \quad (1)$$

$$NDSI = (SWIR - NIR) / (SWIR + NIR) \quad (2)$$

$$NDWI = (R - SWIR) / (R + SWIR) \quad (3)$$

The thematic maps of NDVI, NDSI, and NDWI are shown in Figure 12. The greater NDVI becomes, the more probable it is that the area is covered with vegetation. It is also the case with NDSI for soil and NDWI for water. The results demonstrate clear difference in the indices for the affected areas before and after the tsunami and difference between the affected areas and the other areas after the tsunami. These differences could be good indicators of tsunami inundation. Hence, the analysis on the characteristics of the indices depending on damage states is important for considering the applicability of these indices to tsunami damage detection.

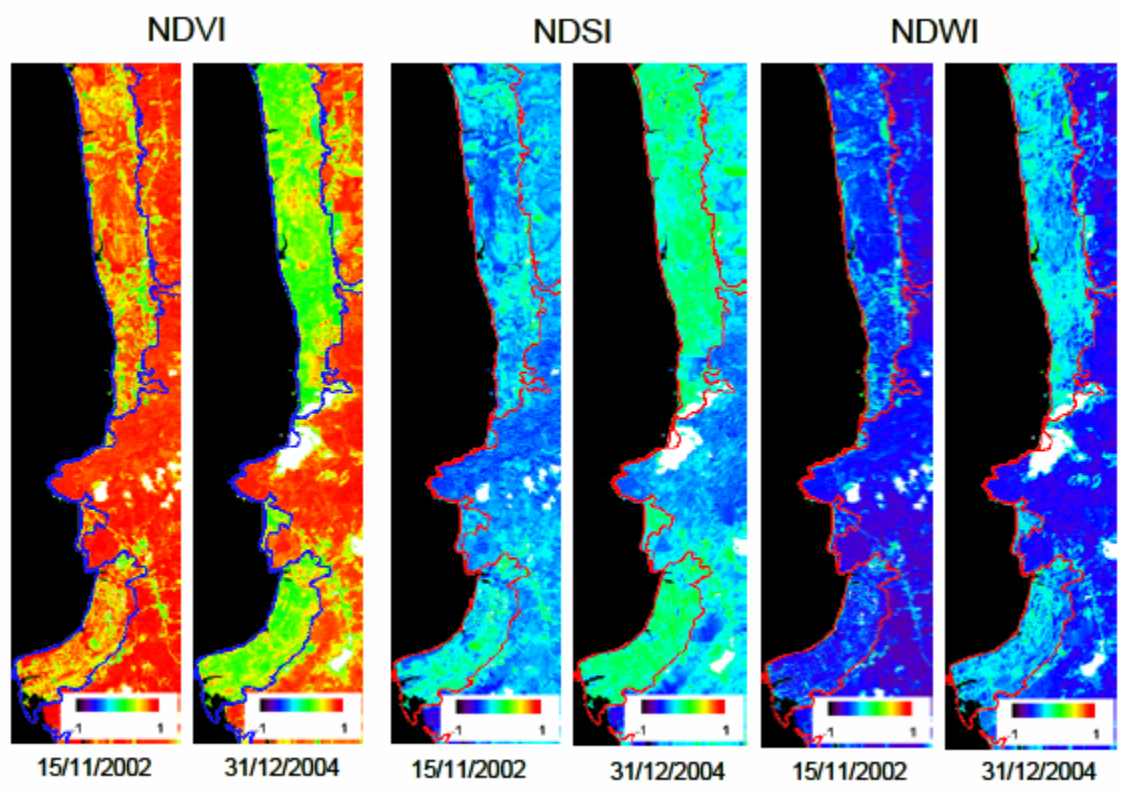

Figure 12. Thematic maps of NDVI, NDSI, and NDWI

Obtaining the distribution of the three indices in the affected areas and the other areas from the data acquired after the tsunami, the ranges of indices that characterize the damage were evaluated. Based on the change of each index before and after the tsunami, the areas affected by the tsunami were identified in the companion paper (Kouchi et al. 2006), after removing the effects of shadow by clouds. The identified areas are in good agreement with the visually detected areas from the pre-event and post-event Ikonos images (Vibulsreth et al. 2005). Although the identified areas include some man-made changes in the period, it can be concluded that moderate-resolution optical satellite images are quite useful to identify tsunami inundation areas.

4. LAND USE CLASSIFICATION OF METRO MANILA, THE PHILIPPINES

Satellite remote sensing, which can easily monitor a large area, could provide effective information to develop building inventory. Multi-spectral characteristics show the difference of reflectance from the materials on the earth surface. Many researchers have already proposed algorithms to classify the features on the earth surface in the fields of natural environment mapping, such as for forests and agricultural lands. However, few studies are found in built environment mapping, although the technology was used to evaluate the thermal environments in urban areas (Ohmachi and Roman 2002). In this study, the classification for understanding seismic vulnerability of Metro Manila, the Philippines, was attempted using Landsat and Ikonos satellite images.

4.1 Macroscopic Land Use Classification using Landsat Images

Multi-spectral sensor of Landsat, Thematic Mapper (TM), has seven bands between visible and thermal infrared. Spatial resolution of its image except for the thermal infrared band is 30m on ground. Three Landsat images, acquired on 26 January 1992 and 16 January 2000, were employed in the land use classification analysis. For gathering the information of old Metro Manila, we also prepared an image acquired on 23 December 1972 by Multi-Spectral Scanner (MSS) of Landsat whose ground resolution is about 80m.

A simple classification for identifying areas of dark object, cloud, and land was carried out using empirical threshold values by multi-level slice technique (Yamazaki et al. 2003). Although there is possibility that the atmospheric and observational effects contained in each image may be different, the selected images actually used here were captured all in winter season. Then, another land cover classification was carried out by using NDVI. Using the Landsat images of Metro Manila for the three time instants, the distribution of categorized NDVI level was calculated. Combination of above-mentioned two classifications (simple and NDVI level), more reliable classification for earth surface information, such as water, dark object, cloud, vegetation and built-up areas, can be derived by using a two-step level slice technique.

Figure 13 shows the classification result by this scheme. In these images, a rapid expansion of urbanized area is clearly observed in this 28-year period. It is noticed that along the Valley (Marikina) Fault system, rapid urbanization is dominant. In this area, the farmlands have been converted to the residential areas. Considering the very short

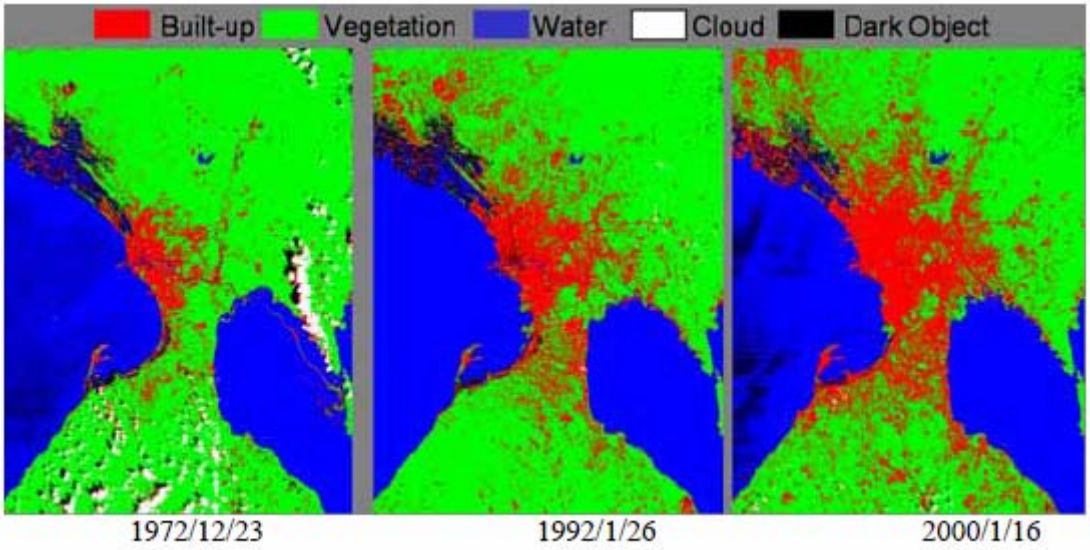

Figure 13 Earth surface classification for Metro Manila estimated by two-step level slice technique from Landsat images in 1972, 1992 and 2000.

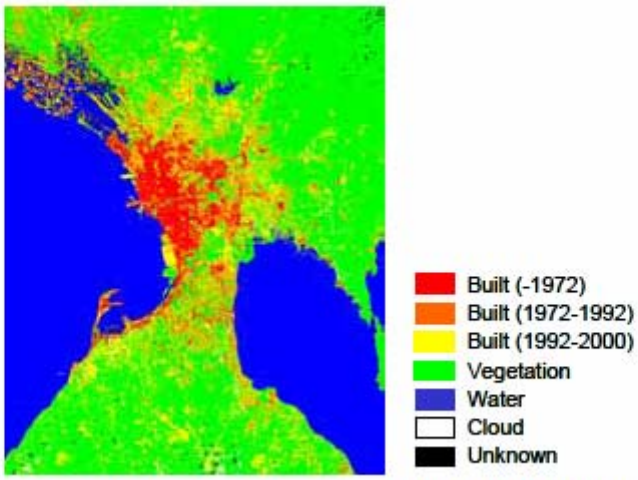

Figure 14. Distribution of estimated built-up age for Metro Manila by time-series analysis

distance to the fault system, the seismic risk of the newly developed areas is considered to be high. It is observed from this figure that the total area of urbanization in Metro Manila is almost equal to that of vegetation in 2000. It is expected that the urban land-use will top vegetation very soon in Metro Manila considering the recent rapid urbanization.

In the Philippines, when evaluating the seismic capacity of buildings, we should consider not only building types, such as concrete hollow block (CHB), RC moment-frame, and RC shear-wall buildings, but also the three design-vintage sub-types; newer buildings (built after 1992), older buildings (built before 1992 but after 1972), and oldest buildings (built before 1972) based on National Structural Code of the Philippines (Pacheco at al. 2003). As the next step of macroscopic analysis using Landsat data, the urbanization areas were further classified based on the building construction age. A built-up age classification image was roughly estimated in

Figure 14 based on Figure 13. In this estimation, we could not count the building-by-building status, because of the coarse resolution of Landsat images and only three limited acquired data. However, this technique and the result may help the macro-grid-scale seismic risk assessment in Metro Manila.

4.2 Microscopic Urban Classification using IKONOS Image

The pansharpened Ikonos image with ground resolution of 1m, which was made by combining the multi-spectral and panchromatic images, was used in this study for Metro Manila. The acquisition date of the Ikonos image is 28 September 2001. The GIS data for Metro Manila, produced in 1986 based on aerial photographs for land use and building information, were also used in the study.

The urban areas in Metro Manila were classified by the level slice method using two indices, NDVI and the texture for the uniformity of digital numbers in a local area. The angular second moment, Ta in Equation 4 derived from a co-occurrence matrix, was used as the texture for the uniformity.

$$Ta = \sum_{m=0}^{m-1} \sum_{m=0}^{m-1} \{P(k,l)\}^2 \qquad (4)$$

An co-occurrence probability P(k, l) means the probability that a pixel value l appears in a relative position δ=(r, θ) from the reference pixel value k, where r and θ of δ are the relative distance and direction from the reference pixel, respectively. m is a grade of an object image used in calculating the matrix. Before the matrix was calculated, the object image was converted to 4-bits. Therefore, m is equal to 16. The angular second moment, Ta, was calculated for the condition of r=1, which indicates neighboring eight pixels around a reference pixel and four directions of “0 or 180”, “45 or 225”, “90 or 270”, and “135 or 315” degrees. The maximum value for the directions was defined as the representative value of the texture. A window size used for the texture analysis on the uniformity in a local area was 51x51 pixels for the Ikonos image. If the texture in a local area is uniform, the angular second moment has a relatively large value.

Using Ikonos data, the classification of built environment in Old Manila was carried out. Each training data of 4,000 pixels was randomly selected from the typical area designated as an inscribed circle, such as a dense area with low-rise buildings, an upscale residential area, an area with mid-height buildings (such as a southern part of Chinatown), and a highly urbanized area with high-rise buildings, and so on.

The edge intensity was derived from Prewitt filter, after the image was fabricated from the method to obtain the brightness signal for NTSC, which is one of the image transmitting systems used for television. Then, the cumulative relative frequency of the edge intensity for the dense area with low-rise small buildings was converted to 4-bits data, by means of dividing an accumulated ratio into 16 equal parts. The angular second moment, Ta, was calculated from the 4-bits edge intensity. As a result, it is found that a high-density area with low-rise buildings has small Ta value, representing the degree of built-up density.

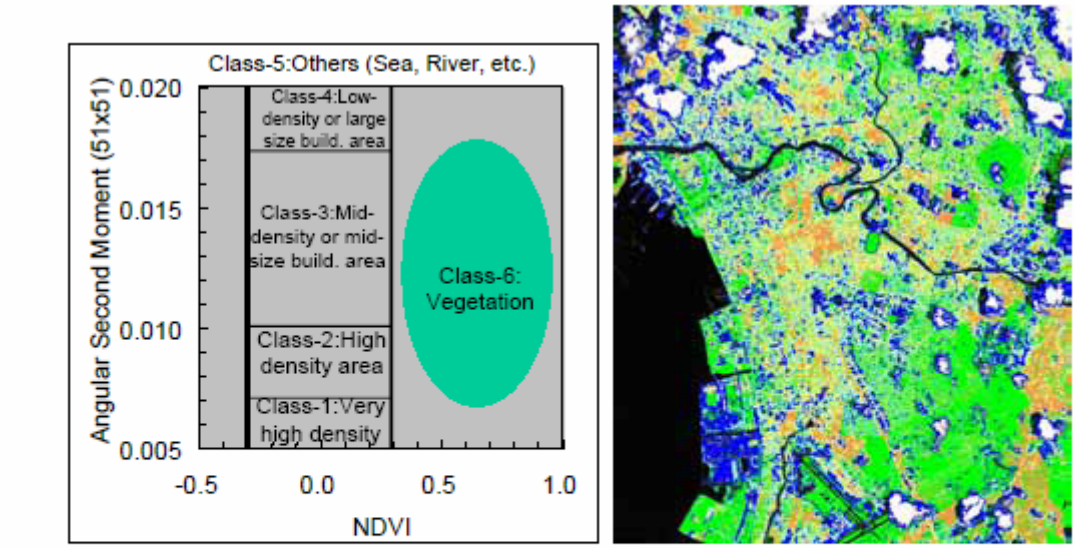

Figure 15 (a) Urban classification in terms of NDVI and texture used for the level slice method and (b) result of microscopic classification in Old Manila using pansharpened Ikonos Image; orange: very high-density area, yellow: high-density area, light blue: mid-density or mid-size building area, blue: low-density or large size building area, green: vegetation area, and black: others.

The classification category for the Ikonos image was determined as shown in Figure 15(a) based on a scatter diagram for NDVI and Ta for training data. Then the level slice classification was carried out and the result is shown in Figure 15(b). It is seen in the figure that many high-density areas with low-rise buildings exist in the east and southeast of Old Manila, such as Pandacan and San Andres. Commercial areas with moderate size buildings locate in the south of Chinatown. The result for low-density or large-scale building areas, such as Makati and Mandaluyong, seems to be relatively in good agreement with the actual situation. On the whole, the result is relatively in good agreement with the actual built environment, except for the areas affected by clouds.

It can be pointed out that the conventional pixel-based image classification methods may encounter some difficulty when they are applied to high-resolution satellite images because one object may be classified into several classes. For example, a road area may be divided into several classes because of the different color of pavement, shadows, cars, etc. Then the classified result of a high-resolution image becomes very noisy. To overcome this kind of difficulty in urban classification using high-resolution images, object-oriented classification is suggested. Examples of object-oriented land cover classification are found in Vu et al. (2005b) for Ho Chi Minh City, Vietnam and in Vu et al. (2005c) for Bam City, Iran.

6. CONCLUSIONS

The use of remote sensing technologies in disaster management is highlighted in this paper, notably post-earthquake/tsunami damage detection due to the 2003 Bam Earthquake and the

2004 Indian Ocean Tsunami, and seismic risk assessment based on land use classification for Metro Manila, the Philippines.
QuickBird (QB) images taken before and after the 26 December 2003 Bam Earthquake were used in visual damage interpretation based on the European Macroseismic Scale building by building. An automated damage detection method was also applied to the post-event Ikonos and QB images. The results of these damage inspections were compared with field survey data and the accuracy and limitation of visual and automated damage detections were presented.

A reconnaissance survey was carried out in south Thailand by a team consisting of researchers from Thailand, Japan, and USA. The primary objective of the survey is to gather geo-referenced tsunami inundation and damage information with the enhanced use of satellite images and GPS. Digital photos and videos were taken in the hard-hit areas and they were linked to the satellite maps. Such perishable data will be invaluable for future research in evaluating damage from tsunami hazards. Terra-ASTER images were used to identify tsunami inundation areas. Three indices to represent land cover characteristics, NDVI, NDSI and NDWI, were employed. Through the analysis on these indices, it is observed that the tsunami caused the decrease of NDVI and the increase of NDSI and NDWI.

A method to develop building inventory is being sought using remotely sensed data. For the first step to evaluate seismic vulnerability of Metro Manila, land use classification was carried out and the expansion of urban areas was observed using time series Landsat images. Ikonos image was also employed for microscopic urban modeling of Metro Mania. Using NDVI and the texture of the image, a detailed classification of urban areas with respect to the density and height of buildings was sought.

REFERENCES

Adams, B.J., Huyck, C.K., Mansouri, B. et al. (2004) The Bam (Iran) earthquake of December 26, 2003: Preliminary reconnaissance using remotely sensed data and the VIEWS system, MCEER Earthquake Reconnaissance Investigation Report, 10p. http://mceer.buffalo.edu/research/Bam/page1.asp

Earthquake Disaster Mitigation Research Center (EDM) (2000) Report on the Kocaeli, Turkey Earthquake of August 17, 1999, The 1999 Turkey Earthquake Report, EDM Technical Report, No. 6, p. 67.

Eguchi, R.T., Huyck, C.K. Houshmand, B., Mansouri, B., Shinozuka, M., Yamazaki, F., and Matsuoka, M. (2000) The Marmara Earthquake: A View from Space, The Marmara, Turkey Earthquake of August 17, 1999: Reconnaissance Report, Technical Report MCEER-00-0001, pp. 151-169.

European Seismological Commission (1998) European Macroseismic Scale 1998.

Ghosh, S., Huyck, C.K., Adams, B.J., Eguchi, R.T., Yamazaki, F., and Matsuoka, M. (2005). Preliminary Field Report: Post-Tsunami Urban Damage Survey in Thailand, Using the VIEWS

Reconnaissance System, http://mceer.buffalo.edu/

Hisada, Y., Shibayama, A., and Ghayamghamian, M.R. (2005) Building damage and seismic intensity in Bam City from the 2003 Iran, Bam, Earthquake, Bulletin of Earthquake Research Institute, University of Tokyo, Vol. 79, No. 3 & 4, pp. 81-94.

Jet Propulsion Laboratory (2005). Shuttle Radar Topography Mission (SRTM), http://www2.jpl.nasa.gov/srtm/index.html

Kouchi, K., Yamazaki, F., Matsuoka, M. (2006) Tsunami Damage Detection Using Moderate-Resolution Satellite Imagery, The 2nd Asian Conference on Earthquake Engineering, CDROM, 11p.

Mitomi, H., Yamazaki, F., & Matsuoka, M. (2000). Automated detection of building damage due to recent earthquakes using aerial television images. The 21st Asian Conference on Remote Sensing, pp.401-406.

Mitomi, H., Saita, J., Matsuoka, M., & Yamazaki, F. (2001). Automated damage detection of buildings from aerial television images of the 2001 Gujarat, India earthquake. IEEE 2001 International Geoscience and Remote Sensing Symposium, CD-ROM. 3p.

Mitomi, H., Matsuoka, M., and Yamazaki, F. (2002). Application of automated damage detection of buildings due to earthquakes by panchromatic television images, The 7th US National Conference on Earthquake Engineering, CD-ROM, 10p.

Ohmachi, T. and Roman, R. E. (2002) Metro Manila, in search of a sustainable future, University of the Philippines Press, 388p.

Pacheco, B. M. et al. (2003) Method of Survey of Local Experts' Judgment on Seismic Capacity of Selected Building Types in Metro Manila, Philippines, Proc. of 5th EqTAP Workshop, CDROM.

Relief Web (2004) http://www.reliefweb.int/w/map.nsf/Emergency?OpenForm&Query=Iran%3A+Earthquake+ -+Dec+2003

Relief Web (2005) http://www.reliefweb.int/rw/RWB.NSF/db900SID/EVIU-6AJJ3C?OpenDocument&rc=3&cc=tha

Takeuchi, W., and Yasuoka, Y. (2004) Development of normalized vegetation, soil and water indices derived from satellite remote sensing data, Journal of the Japan Society of Photogrammetry and Remote Sensing, Vol. 43, No. 6, pp. 7-19 (in Japanese).

Vibulsreth, S., Ratanasermpong, and S., Polngam, S. (2005) Tsunami Disasters along the Andaman Sea, Thailand, Asian Journal of Geoinformatics, Vol. 5, No. 2, pp. 3-15.

Vu, T. T., Matsuoka, M., and Yamazaki, F. (2005a). Detection and Animation of Damage Using Very High-Resolution Satellite Data Following the 2003 Bam, Iran, Earthquake, Earthquake Spectra, Vol.21, No. S1.
Vu, T. T., Matsuoka, M., and Yamazaki, F. (2005b) Object-based Extraction of Buildings from Very High Resolution Satellite Images: A Case Study of Ho Chi Minh City, Viet Nam, Proc.

26th Asian Conference on Remote Sensing, CD-ROM, 5p.

Vu, T. T., M. Matsuoka, and F. Yamazaki, F. (2005c) Towards object-based damage detection. Proceeding of ISPRS workshop DIMAI'2005, Bangkok, Thailand, DVD-ROM, 5p.

Yamaguchi, Y., Kahle, A.B., Pniel, M., Tsu, H., and Kawakami, T. (1998) Overview of Advanced Spaceborne Thermal Emission and Reflection Radiometer (ASTER). IEEE Transactions on Geoscience and Remote Sensing, 36 (4), pp. 1062-1071.

Yamazaki, F., Mitomi, H., Yusuf, Y., and Matsuoka, M. (2003) Urban Classification of Metro Manila for Seismic Risk Assessment using Satellite Images, Fifth Multi-lateral Workshop on Development of Earthquake and Tsunami Disaster Mitigation Technologies and Their Integration for the Asia-Pacific Region, EDM Technical Report, No. 16, CD-ROM.

Yamazaki, F., Kouchi, K., Matsuoka, M., Kohiyama, M., and Muraoka, N. (2004) Damage Detection from High-resolution Satellite Images for the 2003 Boumerdes, Algeria Earthquake, Proceedings of the 13th WCEE, CD-ROM, Paper No. 2595, 13p.

Yamazaki, F., Matsuoka, M., Warnitchai, P., Polngam, S., and Ghosh, S. (2005) Tsunami Reconnaissance Survey in Thailand Using Satellite Images and GPS, Asian Journal of Geoinformatics, Vol. 5, No. 2, pp. 53-61.

ABOUT THE AUTHORS

Fumio Yamazaki is Professor of Urban Environment Systems, Faculty of Engineering, Chiba University, Japan. E-mail: yamazaki@tu.chiba-u.ac.jp

Masashi Matsuoka is Team Leader of Earthquake Disaster Mitigation Research Center (EDM), NIED, in Kobe, Japan. E-mail: matsuoka@edm.bosai.go.jp

ACKNOWLEDGEMENT

The research outputs introduced in this paper have been produced by Dr. T. T. Vu of Earthquake Disaster Mitigation Research Center (EDM), Mr. K. Kouchi of University of Tokyo, and Mr. Y. Yano of Chiba University. Their contributions are deeply appreciated. The field survey data of Bam, Iran, was provided from Prof. Y. Hisada and Mr. A. Shibayama of Kogakuin University, Tokyo, Japan. The visual damage detection result of tsunami-affected areas in Thailand was provided by Ms. Supapis Polngam, GISTDA, Thailand. QuickBird and Ikonos are owned by DigitalGlobe Inc. and Space Imaging Inc., respectively. QuickBird images used in this study were licensed and provided by Earthquake Engineering Research Institute (EERI), Oakland, California, USA. Ikonos image was used in collaboration with Remote Sensing Technology Center of Japan (RESTEC).